Phase-locked arrays of surface-emitting graded-photonic-heterostructure terahertz semiconductor lasers

Yacine Halioua,[1] Gangyi Xu,[1,2,5] Souad Moumdji,[1] Lianhe Li,[3] Jingxuan Zhu,[3] Edmund H. Linfield,[3] A.Giles Davies,[3] Harvey E. Beere,[4] David A. Ritchie,[4] and Raffaele Colombelli[1,*]

[1]*Institut d'Electronique Fondamentale, Univ. Paris Sud, UMR8622 CNRS, 91405 Orsay, France*
[2]*Key Laboratory of Infrared Imaging Materials and Detectors, Shanghai Institute of Technical Physics, Chinese Academy of Sciences, Shanghai 200083, China*
[3]*School of Electronic and Electrical Engineering, University of Leeds, Woodhouse Lane, Leeds LS2 9JT, UK*
[4]*Cavendish Laboratory, University of Cambridge, Cambridge CB3 0HE, UK*
[5]*gangyi.xu@mail.sitp.ac.cn*
[*]*raffaele.colombelli@u-psud.fr*

Abstract: We have demonstrated that a hybrid laser array, combining graded-photonic-heterostructure terahertz semiconductor lasers with a ring resonator, allows the relative phase (either symmetric or anti-symmetric) between the sources to be fixed by design. We have successfully phase-locked up to five separate lasers. Compared with a single device, we achieved a clear narrowing of the output beam profile.

OCIS codes: (140.5965) Semiconductor lasers, quantum cascade; (140.3290) Laser arrays; (140.3070) Infrared and far-infrared lasers; (140.7270) Vertical emitting lasers.

References and links

1. C. Balanis, "Antenna theory: A review," Proc. IEEE **80**(1), 7–23 (1992).
2. D. Botez and G. Peterson, "Modes of phase-locked diode-laser arrays of closely spaced antiguides," Electron. Lett. **24**(16), 1042 (1988).
3. J. B. Khurgin, I. Vurgaftman, and J. R. Meyer, "Analysis of phase locking in diffraction-coupled arrays of semiconductor lasers with gain/index coupling," IEEE J. Quantum Electron. **41**(8), 1065–1074 (2005).
4. C. Sirtori, S. Barbieri, and R. Colombelli, "Wave engineering with THz quantum cascade lasers," Nat. Photonics **7**(9), 691–701 (2013).
5. S. Fathololoumi, E. Dupont, C. W. I. Chan, Z. R. Wasilewski, S. R. Laframboise, D. Ban, A. Mátyás, C. Jirauschek, Q. Hu, and H. C. Liu, "Terahertz quantum cascade lasers operating up to ~ 200 K with optimized oscillator strength and improved injection tunneling," Opt. Express **20**(4), 3866–3876 (2012).
6. K. Unterrainer, R. Colombelli, C. Gmachl, F. Capasso, H. Y. Hwang, A. M. Sergent, D. L. Sivco, and A. Y. Cho, "Quantum cascade lasers with double metal-semiconductor waveguide resonators," Appl. Phys. Lett. **80**(17), 3060 (2002).
7. Y. Chassagneux, Q. J. Wang, S. P. Khanna, E. Strupiechonski, J.-R. Coudevylle, E. H. Linfield, A. G. Davies, F. Capasso, M. A. Belkin, and R. Colombelli, "Limiting Factors to the Temperature Performance of THz Quantum Cascade Lasers Based on the Resonant-Phonon Depopulation Scheme," IEEE Trans. THz Sci. Technol. **2**(1), 83–92 (2012).
8. S. Kohen, B. S. Williams, and Q. Hu, "Electromagnetic modeling of terahertz quantum cascade laser waveguides and resonators," J. Appl. Phys. **97**(5), 053106 (2005).
9. W. Maineult, P. Gellie, A. Andronico, P. Filloux, G. Leo, C. Sirtori, S. Barbieri, E. Peytavit, T. Akalin, J.-F. Lampin, H. E. Beere, and D. A. Ritchie, "Metal-metal terahertz quantum cascade laser with micro-transverse-electromagnetic-horn antenna," Appl. Phys. Lett. **93**(18), 183508 (2008).
10. M. I. Amanti, G. Scalari, F. Castellano, M. Beck, and J. Faist, "Low divergence Terahertz photonic-wire laser," Opt. Express **18**(6), 6390–6395 (2010).
11. J. A. Fan, M. A. Belkin, F. Capasso, S. Khanna, M. Lachab, A. G. Davies, and E. H. Linfield, "Surface emitting terahertz quantum cascade laser with a double-metal waveguide," Opt. Express **14**(24), 11672–11680 (2006).
12. S. Kumar, B. S. Williams, Q. Qin, A. W. Lee, Q. Hu, and J. L. Reno, "Surface-emitting distributed feedback terahertz quantum-cascade lasers in metal-metal waveguides," Opt. Express **15**(1), 113–128 (2007).
13. L. Mahler, A. Tredicucci, F. Beltram, C. Walther, J. Faist, H. E. Beere, and D. A. Ritchie, "High-power surface emission from terahertz distributed feedback lasers with a dual-slit unit cell," Appl. Phys. Lett. **96**(19), 191109 (2010).

#228557 - $15.00 USD Received 4 Dec 2014; revised 13 Feb 2015; accepted 13 Feb 2015; published 6 Mar 2015

14. G. Xu, R. Colombelli, S. P. Khanna, A. Belarouci, X. Letartre, L. Li, E. H. Linfield, A. G. Davies, H. E. Beere, and D. A. Ritchie, "Efficient power extraction in surface-emitting semiconductor lasers using graded photonic heterostructures," Nat. Commun. **3**, 952 (2012).
15. G. Xu, L. Li, N. Isac, Y. Halioua, A. Giles Davies, E. H. Linfield, and R. Colombelli, "Surface-emitting terahertz quantum cascade lasers with continuous-wave power in the tens of milliwatt range," Appl. Phys. Lett. **104**(9), 091112 (2014).
16. E. Istrate and E. Sargent, "Photonic crystal heterostructures and interfaces," Rev. Mod. Phys. **78**(2), 455–481 (2006).
17. G. M. de Naurois, M. Carras, G. Maisons, and X. Marcadet, "Effect of emitter number on quantum cascade laser monolithic phased array," Opt. Lett. **37**(3), 425–427 (2012).
18. C. Zmudzinski, D. Botez, and L. Mawst, "Simple description of laterally resonant, distributed feedback like modes of arrays of antiguides," Appl. Phys. Lett. **60**(9), 1049–1051 (1992).
19. D. Botez, L. Mawst, and G. Peterson, "Resonant leaky-wave coupling in linear arrays of antiguides," Electron. Lett. **24**(21), 1328 (1988).
20. T.-Y. Kao, Q. Hu, and J. L. Reno, "Phase-locked arrays of surface-emitting terahertz quantum-cascade lasers," Appl. Phys. Lett. **96**(10), 101106 (2010).
21. S. Barbieri, J. Alton, H. E. Beere, J. Fowler, E. H. Linfield, and D. A. Ritchie, "2.9 THz quantum cascade lasers operating up to 70 K in continuous wave," Appl. Phys. Lett. **85**(10), 1674 (2004).
22. D. Botez, A. P. Napartovich, and C. Zmudzinski, "Phase-locked arrays of antiguides: analytical theory II," IEEE J. Quantum Electron. **31**(2), 244–253 (1995).

1. Introduction

The phasing of individual electromagnetic sources, namely the ability to control the relative phase of the emission emitted from each source, underpins a broad range of important phenomena. For example, if the distance between sources is less than the wavelength, beam-steering can be achieved without the need for any mechanically moving parts. If, however, the distance between the sources is larger than the wavelength, then the directionality of the ensemble emission can be enhanced. But in both cases, it is essential to have a fixed relative phase between each source.

Phased arrays of sources emerged naturally in the radio-frequency domain, since the phase of each radiating antenna is directly linked to the phase of the supplied current [1]. Phasing optoelectronic devices operating at optical/infrared wavelengths is far more complex, however, since phases in individual devices cannot be controlled electronically. One can create coherent super-modes distributed over an array by weakly coupling devices (for example, by leakage-coupling [2], radiative coupling [3], or directly through the use of couplers). But, in this configuration, the real challenge is to select specific modes among the many competing alternatives, since only specific sub-sets of emitted super-modes will directly match the desired application. For example, to increase the beam directionality of an ensemble of N sources, the ideal configuration is to have a totally symmetric overall state, in which all sources exhibit the same phase. This illustrated in Fig. 1 for a prototypical case of the far-field emission pattern of surface-emitting THz frequency semiconductor lasers. For two sources, the phased configuration provides a narrower central-lobe in the far field emission profile. However, the anti-phased configuration yields a bi-lobed pattern that is unlikely to be suitable for most common applications. As the number of sources is increased (e.g. to N = 5), the fully symmetric solution begins to provide a markedly narrower central lobe.

The THz frequency quantum cascade (QC) laser is a particularly important candidate for such studies, as there is a need for efficient and powerful sources in this part of the electromagnetic spectrum [4]. QC lasers are electrically-injected semiconductor sources that can emit across the mid-infrared and THz spectral regions using heterostructures based on highly developed III–V semiconductor materials.

The highest recorded maximum operating temperature T_{max} (currently 200 K) [5], for THz QC lasers have been obtained using metal–metal waveguides [6,7] and, as such, international efforts to increase the output power have focused on this waveguide architecture, although the superior temperature performance comes at the price of poor extraction efficiency [8]. A number of effective metal-metal waveguide designs have, however, been recently developed and show state-of-art performance (in terms of threshold current density and T_{max}) for both edge emission [9,10] and surface emission [11,12,13]. Amongst these, the graded photonic

#228557 - $15.00 USD Received 4 Dec 2014; revised 13 Feb 2015; accepted 13 Feb 2015; published 6 Mar 2015

heterostructure (GPH) concept demonstrated in [14] has led to powerful surface emission, both pulsed and continuous wave (CW), with a single lobed and low divergent (albeit elliptical) output beam [15]. The core concept of GPH resonators is separate confinement for the radiative and non-radiative modes. The grating period is not constant, rather, it is graded to mimic a type-II potential well for photons [16]. Such a resonator localizes the symmetric/radiative modes in the device centre, whilst positioning the anti-symmetric/non-radiative modes close to the lossy laser facets, as described in [14].

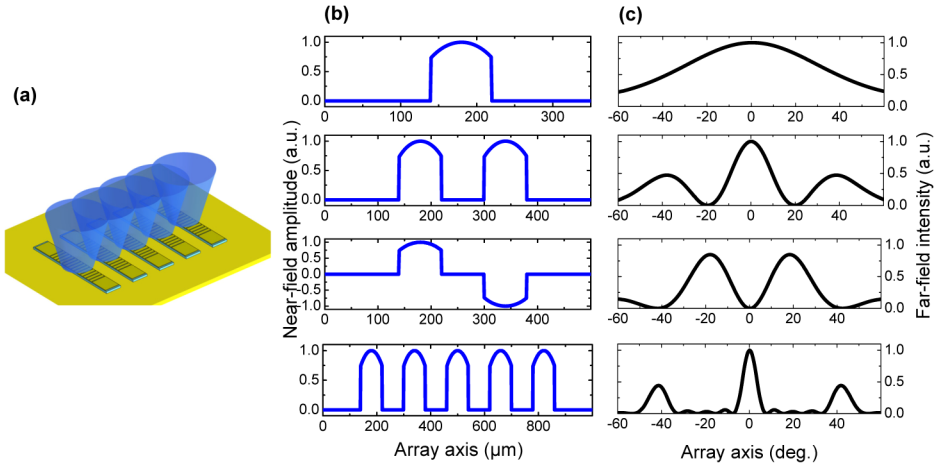

Fig. 1. Phase-locking surface-emitting THz-QC lasers with GPH resonators. (a) Schematic diagram of an array containing five GPH lasers. (b) Near-field amplitude profiles in various configurations along the array (vertical) axis. From top to bottom: single GPH; arrays containing two GPH lasers which are in phase and in anti-phase; and, an array with five in-phase GPH lasers. (c) Resulting far-field profiles along the array axis, corresponding to the near-field profiles given in (b). Depending on the relative phase of the laser elements, the emission exhibits a node or a maximum in the vertical direction. The central peak becomes narrower as more laser elements are locked together in-phase.

In this work we use GPH devices as building blocks in phase-locked arrays. Increasing the device surface area tends to reduce the individual device performance since it leads to elevated thermal loads, and/or multi-mode behaviour. But, we show here that if a deterministic relative phase can be imposed upon devices in an array, then one can reduce the beam divergence and increase the output power by increasing the *effective* device emission surface. This cannot be achieved using evanescent coupling [17] or leaky-wave coupling *via* an antiguide configuration [18,19] given the extreme confining properties of metal-metal waveguides. Note however that Kao *et al.* demonstrated a phase-locked array (up to 6 elements) of THz second-order, low-output-power DFB lasers using propagating wave coupling, i.e. by joining one edge of each laser with a curved waveguide coupler [20]. We explore in this paper a different approach since this configuration appears of difficult application to phase-locking GPH lasers, since the lasing modes are strongly localized in the device centre.

2. Design

In order to induce a stable and fixed relative phase between the GPH lasers, we use a hybrid array configuration: the GPH lasers are embedded into a larger ring resonator which sets the mode symmetry. The principle is shown schematically in Fig. 2(a) (for two lasers). The GPH laser wavelengths (λ_{GPH}) are determined by their metallic gratings. The ring resonator – with the curved parts left electrically un-pumped – then supports a series of odd/even ring modes whose wavelengths are given by $\lambda_{ring} = n_{eff} \cdot L/m$, where L and n_{eff} are respectively the total length and effective index of the ring resonator, respectively, and m is an odd/even number.

#228557 - $15.00 USD Received 4 Dec 2014; revised 13 Feb 2015; accepted 13 Feb 2015; published 6 Mar 2015

Given the geometric symmetry of the ring, the field distribution in the two straight sections is either in-phased (even mode) or anti-phased (odd-mode).

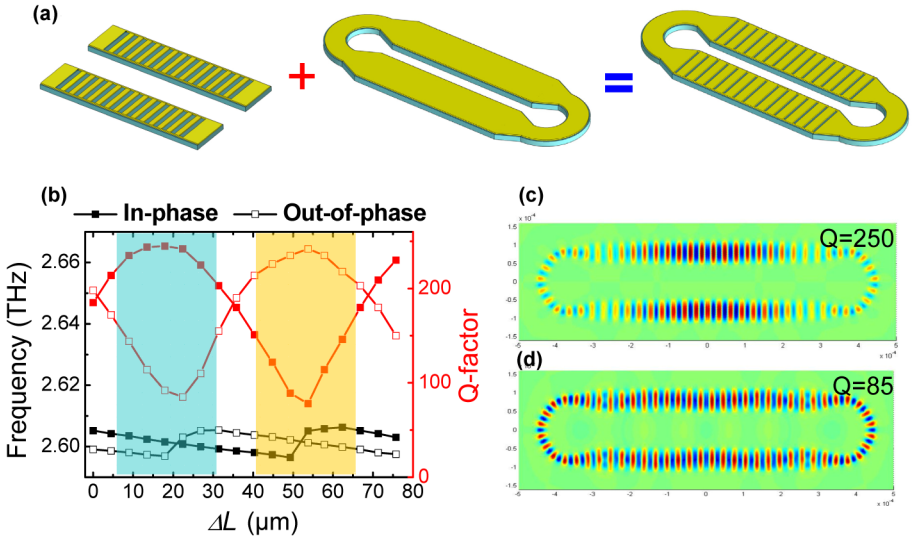

Fig. 2. Simulations of phased arrays containing two GPH lasers. (a) Conceptual diagram showing a phase-locked array of two GPH lasers. Two identical GPH lasers are embedded into a ring resonator: the GPH grating determines the emission wavelength, whilst the ring sets the field symmetry and hence the phase relationship between the two lasers. (b) Influence of the relative ring length (ΔL) on the frequency and Q-factors of the two relevant optical modes in the array: the symmetric and anti-symmetric modes, respectively. The lines with solid squares correspond to the symmetric mode, the lines with open squares to the anti-symmetric mode. The black plots correspond to the frequency, the red to the Q-factors. As ΔL varies, the frequencies of the symmetric and anti-symmetric modes alternatively match the GPH frequency, and therefore exhibit a high Q-factor favouring lasing. Typical examples are shown in panels (c) and (d), where the field distributions of two modes are plotted, showing the character of a GPH mode in anti-phase with high Q-factor (c)), and the character of ring mode in-phase with low Q-factor (d).

The free spectral range (λ_{SPR}) and the spectral line width ($\Delta\lambda$) of the ring modes are determined *by design* of the total ring length and the length of the un-pumped parts, respectively. The design strategy is to set the free spectral range roughly twice the spectral width of each ring mode, i.e. $\lambda_{SPR} \approx 2 \times \Delta\lambda$. It follows that one ring mode only always overlaps with the GPH mode spectrally. This near-resonant mode is mainly bound to the GPH zones, and its Q-factor is high. The other modes, on the other hand, which are not resonant with the GPH mode, provide a uniform field distribution along the ring. This results in Q-factors significantly less than the GPH mode, since the un-pumped parts induce high losses.

FDTD simulations (Figs. 2(b)-(d)) provide an insight into this phenomena. The simulations have been performed with the commercial code Lumerical. We investigate – when the total ring length changes by a value ΔL – the evolution of the Q-factor, and the frequency of the two relevant modes (symmetric and anti-symmetric, respectively) in the hybrid resonator. Figure 2(b) shows that, by changing ΔL, the GPH mode alternately overlaps with an odd or even ring mode, leading to a periodic oscillation of the frequency and Q-factor of the symmetric and anti-symmetric modes. For example, when an odd ring mode is in resonance with the GPH mode, which means that their frequencies are very close, simulations show that the electromagnetic field is mainly confined in the GPH sections. This results in a high Q-factor, as shown in the Fig. 2(c). In contrast, when the frequency of a ring mode (even mode, for example) is not in resonance with that of the GPH mode, simulations show that the mode is less localized in the GPH sections. Instead, the electromagnetic field is nearly uniformly distributed along the whole resonator. This results in a low Q-factor, because the

#228557 - $15.00 USD Received 4 Dec 2014; revised 13 Feb 2015; accepted 13 Feb 2015; published 6 Mar 2015

curved parts are not pumped and exhibit elevated losses, as shown in Fig. 2(d). Fig. 2(b) highlights that, given the large difference in Q-factors, the mode competition is won either by the symmetric GPH-like mode (blue shaded region), or by the anti-symmetric mode (orange shaded region) for a large range of ΔL values. This provides a stable scheme to phase-lock two GPH lasers.

3. Experimental results: phased arrays of two THz lasers

We demonstrated this operating principle experimentally using a phased array of two THz surface emitting lasers (Fig. 3), where the relative length of the ring ΔL is the tunable parameter. The fabrication steps are similar to those for a single GPH [15], and the laser active region is based on a bound-to-continuum design [21] (samples V414 and L870). Figure 3 shows the results from two laser arrays operating in phased/anti-phased mode, respectively; these will serve as basis for this discussion. We tested 8 devices with values of ΔL changing gradually from 14 μm to 64 μm. We found that 6 devices over 8 operate in a phased/anti-phased configuration. For ΔL values between 14 μm to 30 μm, the laser arrays operate in phased mode. On the other hand, for ΔL values between 42 μm to 58 μm, the arrays operate in anti-phased mode. For only two values of ΔL, 34 μm and 64 μm, the array is not phased. These results are in good agreement with the calculations given in Fig. 2(a), confirming the robustness of the phasing approach. The corresponding data (1D far-field scans) are reported in Fig. 4. All the far-field measurements have been acquired by scanning a Golay cell on a sphere at constant radius (between 10 cm and 15 cm) from the laser surface.

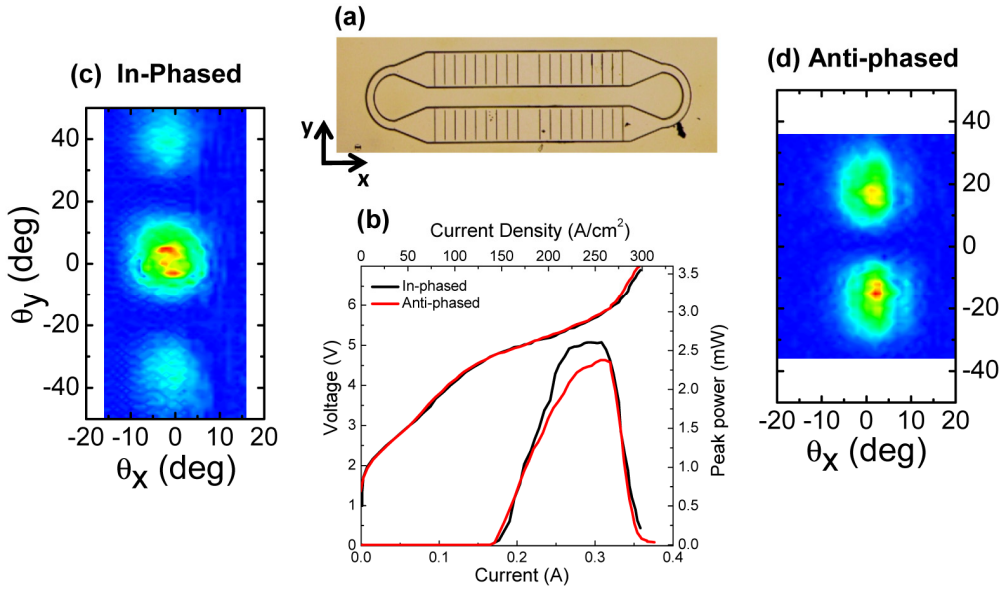

Fig. 3. Performance of phase-locked arrays containing two GPH lasers. (a) Microscope image of an array containing two GPH lasers. (b) Plot of current density and output power as a function of bias for arrays where the two GPH lasers are in-phase (black) and anti-phase (red). The corresponding far-field emission profiles are presented in (c) and (d), respectively. The far-field profiles were measured in pulsed mode (1μs pulse width, repetition frequency 50kHz) at a heat-sink temperature of 20 K.

The far-field measurements (Figs. 3(c) and 3(d)) provide a clear identification of the lasing modes. First, the single lobe pattern along the GPH axis (x-axis in Fig. 3) proves that the lasers operate correctly on the fundamental radiative mode [14]. Second, the signature of phase-locking of the two surface-emitting lasers is the high-contrast interference profile along the direction perpendicular to the GPH (y-axis in Fig. 3). The two far-field profiles in Figs. 3(c) and 3(d) match the beam patterns obtained from the 1D numerical calculations: two main

#228557 - $15.00 USD Received 4 Dec 2014; revised 13 Feb 2015; accepted 13 Feb 2015; published 6 Mar 2015

lobes and a central node for anti-phased coupling (Fig. 3(d), simulations not shown), or a central peak with two small side-lobes for phased coupling (Fig. 3(c), 1D simulation shown in Fig. 6a). The 1D numerical calculations have been performed by Fourier-transformation of the electromagnetic near-field at the lasers' surface, which was assumed as in Fig. 1(b).

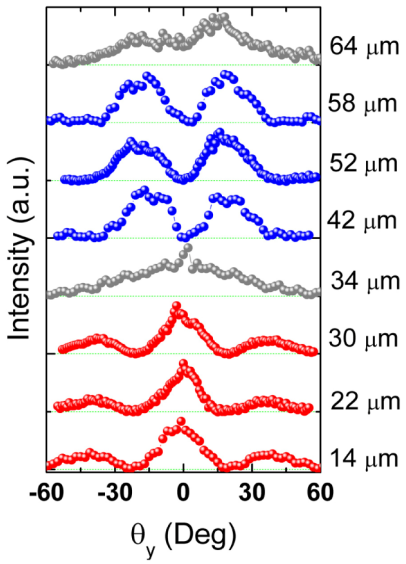

Fig. 4. Stability of the phased array of two surface-emitting GPH THz lasers. Experimental, 1D far-field acquired for several devices with different ΔL lengths. The scans have been acquired across the θ_y direction. It is the direction *orthogonal* to the laser ridges and it allows one to gauge the phased/anti-phased operating mode. Eight devices have been tested, and 6 of them operate in phased or anti-phased mode. These measurements confirm the stability of the phasing mechanism for the phased array of 2 elements.

In both configurations, laser operation is corroborated by the light-voltage-current (LVI) characteristics (Fig. 3(b)). The threshold current density (J_{th}) is ~160 A.cm^{-2}, while the peak output power at 20 K is ~2.5 mW. The output power and J_{th} are identical for both devices. This is expected from a 'weak/perturbative' coupling picture where the intensity adds linearly and the phasing only induces an angular redistribution of intensity (i.e. redistribution in ***k***-*space*). These experiments thus demonstrate that the scheme is suitable for coupling at least two surface-emitting lasers. The individual properties of each GPH unit (single lobed emission and operating on radiative modes) are maintained; the arrays are stable since the majority of the devices we tested operate in phased/anti-phased mode (see Fig. 4). Finally, the phase relationship can be reliably controlled through the relative ring length, *ΔL*.

4. Experimental results: phased arrays of several THz lasers

We now consider arrays with up to five elements (Fig. 5), and focus the discussion on in-*phased* devices only, i.e. where the relative length *ΔL* leads to a main emission lobe which is exactly orthogonal to the device surface. Figures 5(a)-(e) (top) show images of the fabricated single GPH laser and arrays containing two, three, four and five elements. The corresponding far-field emission patterns are also shown, measured at low temperature in pulsed mode. All the devices in array configuration show constructive interference patterns, which is evidence of coupling between the separate GPH units. Furthermore, lasing operation on the radiative mode is always seen, as the emission is single lobed along the GPH direction (x-axis).

#228557 - $15.00 USD Received 4 Dec 2014; revised 13 Feb 2015; accepted 13 Feb 2015; published 6 Mar 2015

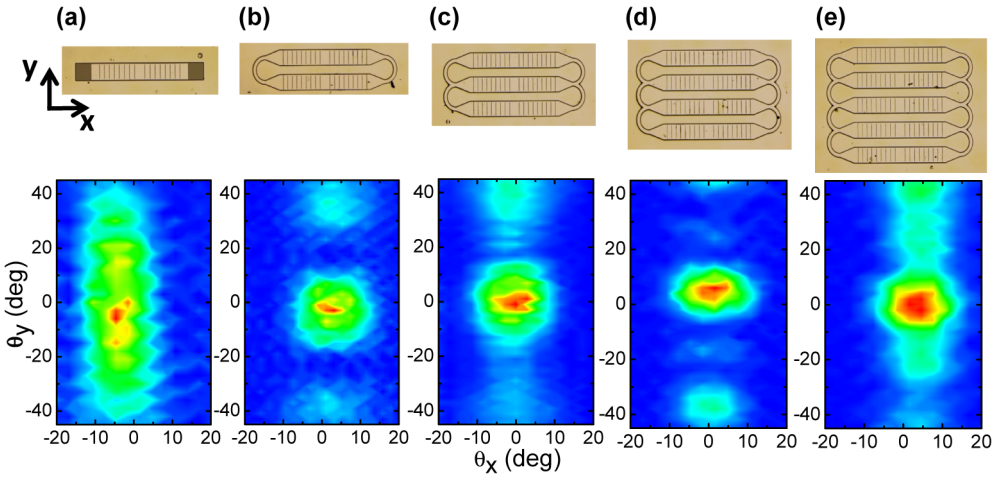

Fig. 5. Far-field emission patterns of arrays containing different number of elements. Microscope (upper) and far-field emission patterns (lower) of a single GPH laser and arrays containing from two up to five laser elements. The devices were measured at an injection current density of ≈300 A/cm^2 (300-ns-wide pulses at a repetition rate of 400 kHz).

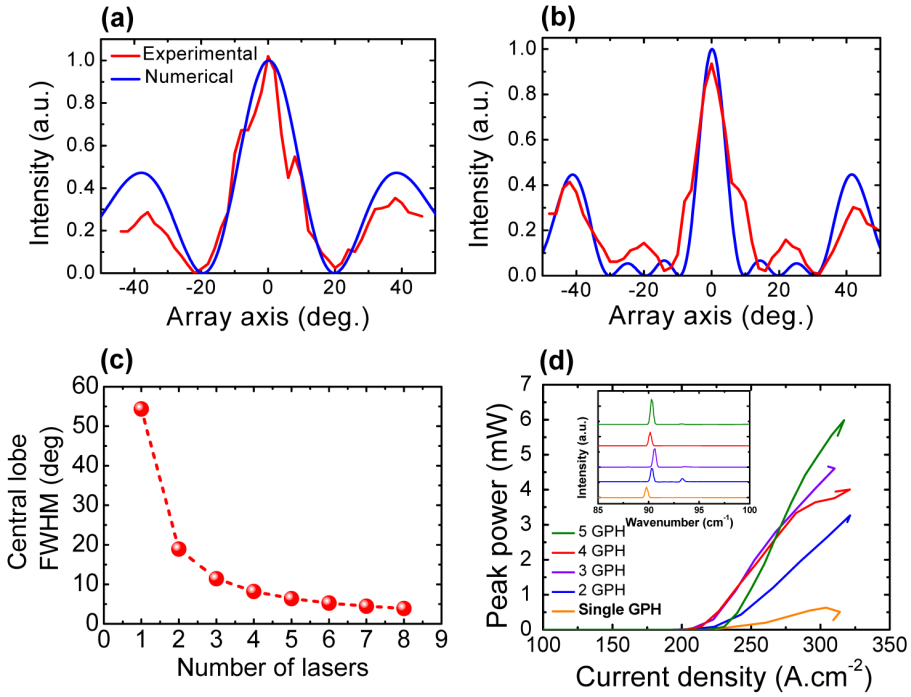

Fig. 6. Scaling of phased arrays with the number of elements: divergence angle, spectra and output power. (a) and (b) show the measured (red curve) and calculated (blue curve) far-field beam profiles along the array axis for two and four in-phased laser elements, respectively. (c) Calculated relationship between the number of elements in the array and the divergence angle (FWHM) of the central lobe. (d) Output power as a function of current density for the single GPH laser and arrays where all the elements are in-phased (devices presented in Fig. 5). The maximum output power scales with the number of elements in the array. Most importantly, the slope efficiency *per unit device* is almost invariant (see Fig. 7). The inset shows the laser emission spectra of the devices at an injection current density of ≈300 A/cm^2. The measurements are performed with 200-ns-wide pulses at a repetition rate of 100 kHz.

#228557 - $15.00 USD Received 4 Dec 2014; revised 13 Feb 2015; accepted 13 Feb 2015; published 6 Mar 2015

Compared with the far-field emission pattern obtained for a single surface-emitting laser (Fig. 5(a)), a clear narrowing of the output beam profile is observed when a second device is added (Figs. 5(b)). Increased sharpening (Figs. 5(c)-(e)), albeit less dramatically, is seen as the number of devices in the array is increased further, with a detailed comparison being given in Figs. 6(a)-(b) for arrays with two and four elements, which are the ones for which the 1D model best fits the experimental data. This is confirmed by the 1D numerical calculations (Fig. 6(c)), which show the angular divergence (full-width at half maximum) of the output beam as a function of the number of GPH elements in the array. After a dramatic initial angular narrowing, the output beam divergence progressively reduces with increasing number of elements. The divergence of a single GPH laser in the direction perpendicular to the ridge is inversely proportional to the width of the field distribution in the near-field along the same direction. On the other hand, the divergence of the array is inversely proportional to the distance between the laser elements located at the edges of the array itself (or, equivalently, to the effective aperture size of the array). This explains the weaker narrowing of divergence angle when the number of elements in the array is increased from two to five. Ultimately, one is limited by the resolution of the apparatus (the far field profiles were acquired with 2 degree steps, with an experimental resolution of 0.6 degrees).

Figure 6(c) suggests that – for this specific architecture - arrays comprising three elements represent a good compromise for potential application of this technique, as they provide: an excellent far-field emission profile, a factor of three increase in power over a single device, and a relatively straightforward device design and fabrication. In fact, as the number of array elements is increased, the appropriate range of ΔL that ensures phased/anti-phased behavior becomes more restricted, and for several values of ΔL the emission is un-phased. Figure 5(e) shows, for example, that the array of five lasers exhibits a strong background signal, demonstrating a non-perfect phased behaviour. We believe that this observation is related to the intrinsic optical properties of the coupled-resonator scheme [22], rather than predominantly being related to lithographic tuning. Figures 6(a)-(b) show that, with certain ring length ΔL, the far-field pattern matches very well the 1D numerical calculations based on antenna theory.

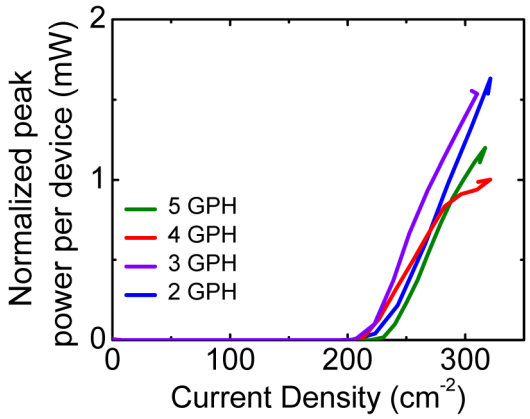

Fig. 7. LI characteristics normalized by the number of devices in the array. The LI characteristics of Fig. 6(d) are presented here normalized by the number of elements in the array. The slope efficiency *per unit device* in the arrays are the same within +/– 5%, except for the array of 4 which is under-performing. The exact values are, in mW/kAcm^{-2}: 17.7 (array of two); 17 (array of 3); 13 (array of 4); 16 (array of 5). This suggests that the performance of each emitting unit in the coupled system is maintained independently of the number of GPH in the array.

For the case of a phased array of several devices, the light-current measurements in Fig. 6(d) show that the output power increases with increasing number of lasers in the array (except for the array of 4 lasers which is under-performing). Most importantly the slope

#228557 - $15.00 USD Received 4 Dec 2014; revised 13 Feb 2015; accepted 13 Feb 2015; published 6 Mar 2015

efficiency (see Fig. 7) scales proportionally with the number of elements in the array (again with the exception of the array of 4 lasers). Importantly, the emission frequency of the lasers (Fig. 6(d), inset) is essentially unaffected by the number of elements in the array. This is further evidence, together with the consistency of J_{th}, that the system operates in a *weak-coupling* regime. We also observed lasing action up to a temperature of 100 K, only 10K below that measured for a QC laser fabricated from the same material in a standard Fabry-Perot metal-metal waveguide configuration. This shows that the implementation of the array is not a major obstacle to the thermal properties of the devices.

5. Conclusions

In conclusion, we have demonstrated an effective way to phase-lock arrays of surface emitting THz QC lasers. Compared with the performance of a single device, we observed a dramatic narrowing of the output beam profile, and a scalability of the output power with the number of elements in the array. We find that arrays comprising three elements represent an optimal trade-off between fabrication complexity and output power/beam profile.

Acknowledgments

This work was partly supported by the French RENATECH network. R.C. acknowledges partial support from the ERC "GEM" grant (Grant Agreement No. 306661) and from the French National Research Agency (ANR-2012-NANO-014 "PHASE-LOCK" and ANR-2011-NANO-020 "DELTA"). G. Xu acknowledges support from "The Hundred Talents Program" of CAS and the "Shanghai Pujiang program" (14PJ1409700). The University of Leeds acknowledges: the EPSRC, the ERC (TOSCA), the Royal Society and the Wolfson Foundation. We would also like to thank Dr Mohammed Salih for his assistance in characterizing material.

#228557 - $15.00 USD Received 4 Dec 2014; revised 13 Feb 2015; accepted 13 Feb 2015; published 6 Mar 2015